Available online at www.sciencedirect.com

ScienceDirect

Ceramics International 42 (2016) 3388–3396

CERAMICS INTERNATIONAL

www.elsevier.com/locate/ceramint

Densification kinetics and anisotropic microstructure evolution in LTCC films constrained by rigid substrate

Shishun Qi, Ruzhong Zuo*, Zhaosheng Ma

Institute of Electro Ceramics & Devices, School of Materials Science and Engineering, Hefei University of Technology, Hefei 230009, PR China

Received 21 August 2015; received in revised form 9 October 2015; accepted 26 October 2015
Available online 30 October 2015

Abstract

LTCC films with thickness of 130 μm were cast on the alumina substrate and the free and constrained sintering behavior was measured by utilizing an optical dilatometer. It was found that constrained films started to densify at a low temperature of 720 °C. The apparent activation energies for free and constrained films were calculated through densification data obtained in the constant-heating-rate experiment. Of particular notice, with increasing density, the activation energy for constrained films decreased from 690 kJ/mol to 359 kJ/mol, whereas a relatively fixed value of 530 ± 30 kJ/mol was yielded for the freely sintered ones. The final density for constrained films was lower than that of the free ones, which could be attributed to the constraint from the substrate. Moreover, anisotropic microstructure was evolved in the constrained film with the increase of density and elongated pores were more prone to align parallel to the substrate.

Keywords: Constrained sintering; LTCC film; Densification kinetics; Anisotropy

1. Introduction

Low temperature co-fired ceramics (LTCC) have been extensively studied over the last decades, possessing great potential in promising areas ranging from wireless communication, sensor technology, electronic control units to microsystems [1–4]. The dimensional accuracy of the LTCC component acts as a critical factor for achieving high performance device, which is highly dependent on the processing engineering [2,3]. It is well known that sintering forms the crucial step in LTCC since mismatched sintering behavior of different components can lead to cracks, warpage, and non-uniform shrinkage, which would lead to poor dimensional tolerances and performance degradation [5–8]. To improve the dimensional accuracy, constrained sintering technologies, mainly consisting of pressure-assisted sintering (PAS) and pressureless-assisted sintering (PLAS) technologies, have been developed and employed frequently in industrial production [9–11]. Particularly, PLAS has been the most utilized technology, in which LTCC films are usually constrained by non-densifying layers, rigid substrates or sacrificial layers. Films deposited on a rigid substrate could realize the tight dimensional accuracy for reliable modules as well as meet some functional requirements, including mechanical, optical and thermal properties [11].

As a typical constrained sintering case, a film constrained by the rigid substrate is not only a conventional feature of many ceramic processing technologies, but also an issue of considerable fundamental interest [6,7,12–23]. Owing to the existence of interfacial friction between the substrate and film, an in-plane tensile stress usually develops during the sintering process. Thus, the in-plane shrinkage is inhibited and all densification takes place only in the thickness direction. The densification behavior of constrained films has been extensively studied both theoretically and experimentally [14–23]. However, a big discrepancy is always observed for the theoretically predicted and experimentally measured densification behaviors, indicating altered densification kinetics in the constrained film [6,7,14,20]. For typical polycrystalline and LTCC films, the actual constrained sintering behavior usually deviates from theoretical predictions, making the research of constrained sintering kinetics difficult to proceed [14,20]. As

*Corresponding author. Tel./fax: +86 551 62905285.
E-mail addresses: piezolab@hfut.edu.cn, rzzuo@hotmail.com (R. Zuo).

http://dx.doi.org/10.1016/j.ceramint.2015.10.133
0272-8842/

found by Kim et al., the apparent activation energy of 3YSZ films is much lower for constrained sintering than for free sintering, owing to the in-plane tensile stress [21]. However, much higher activation energy is obtained for constrained silver and gold films, revealing an altered densification mechanism [6,7]. Therefore, a deep understanding of the LTCC constrained sintering kinetics is earnestly needed to optimize the processing parameters and minimize possible defects. According to previous reports, the changed sintering kinetics for constrained films is closely related with the anisotropic densification behavior and microstructure evolution [6,7,15–23].

It has been well addressed that anisotropic microstructure exerts deep impacts on the viscous properties such as uniaxial viscosities and viscous poisson's ratio [2,4,14,24–26]. However, only several reports illustrate the microstructure evolution under the influence of a geometrical constraint [27–30]. In constrained samples, the microstructure usually deviates from isotropy during the sintering process [24,31]. And the microstructure evolution is implicated in the external stress and the densification mechanism. Pores aligning along the loading direction are observed by Zuo et al. in the sinter-forged Al_2O_3, which could be assigned to the promoted neck growth from the modified diffusional fluxes [31]. Guillon et al. have also demonstrated that pores in constrained Al_2O_3 films became more anisometric with their long axes along the thickness direction, because of the prohibited mass transfer in the in-plane direction [20,29]. However, the case is of great discrepancy for LTCC materials, since they are mostly densified through viscous flow [2,32]. Ollagnier et al. find that pores are more prone to align perpendicular to the external stress in a sinter-forged LTCC sample, which could be attributed to the altered viscous flow during the sintering process [2]. Whereas, there barely exists detailed study on the anisotropy evolution in constrained LTCC films.

Thus, detailed investigations on the constrained densification kinetics and anisotropic microstructure would be of great significance for the increasing LTCC applications. A typical commercial LTCC material, belonging to a glass ceramic system was utilized in the study [33]. Constrained LTCC films were fabricated through the tape casting method and their densification behavior was measured by our lab-made optical dilatometer equipped with a rocking arm. Characterization of microstructural changes was performed by studying pore orientation with the purpose of highlighting any possible development of anisotropy. It is anticipated that the present work would give a better understanding with regard to the influence of the geometrical constraint on the densification kinetics and microstructure evolution in constrained LTCC films.

2. Experimental

LTCC films were fabricated through the tape casting method. Ferro A-6M LTCC powder was used and films with a thickness of 130 μm could be obtained by adopting suitable processing parameters. The films were cast onto fine-grained, high-purity alumina plate and mylar carrier films, respectively. The reference axes are: x for the tape casting direction, y the transverse and z the thickness direction. Then, films on the mylar film were peeled and cut into square pieces of 10 mm × 10 mm. Stacked samples with 15 pieces of film were used as the free film. They were laminated under a uniaxial pressure of 20 MPa at 80 °C for 5 min. For sintering, the same program was applied for both the free and constrained films. The samples were first heated to 450 °C with a slow heating rate of 2 °C/min and held for 2 h in order to burnout the binder completely. Then, they were heated to 760 °C, 780 °C, 800 °C at a heating rate of 10 °C /min and held for 2 h, respectively.

For freely sintered films, the shrinkage occurred in all directions and an optical dilatometer was utilized to record the shrinkage of samples [34]. However, the shrinkage of constrained films only occurred in the thickness direction. Owing to the size limit of constrained films, a quartz rocking arm with a magnification of 20 was designed and employed to facilitate the thickness measurement. The film density after binder burnout was geometrically determined in order to facilitate the instantaneous density calculation through the measured strains. Furthermore, final densities for free films were also determined through the Archimedes method and they were in good agreement with the calculated results.

To characterize the sintering activation energy of the free and constrained film, constant-heating-rate (CHR) experiments were performed and the density evolution as a function of sintering temperature was determined [35]. The films were sintered at heating rates of 2 °C /min, 5 °C /min and 10 °C /min up to a maximum temperature of 850 °C.

To characterize the microstructure, constrained films were fractured in the y–z plane and the freely sintered samples were sliced in half from top to bottom. Each specimen was carefully ground and polished to a 5 μm finish. The polished surfaces were then coated with a thin gold conductive layer for the examination of pore morphologies by the scanning electron microscope (SEM, SSX-550, Shimadzu, Japan). Firstly, constrained film sintered at 780 °C for different time was characterized to explore the pore evolution law. To make the law more obvious, a thinner film with a thickness of 70 μm was used. Then, microstructure of the free and constrained film (130 μm) sintered at different temperatures was also characterized. For each sample, more than 500 pores were selected for analysis by means of ImageJ software (NIH, USA). Micrographs were modified in the following way: contrast enhancement, background subtracting, median filtering and thresholding in order to obtain suitable binary images [28,29]. Some pores have to be manually handled to avoid errors in pore areas. An ellipse of equivalent area was then generated for each pore. The length and angle of equivalent pores were then measured through the image software (Adobe Photoshop CS6, Adobe, USA). Subsequently, the pore orientation was obtained by analyzing the statistical data acquired from images and the anisotropy evolution could thus be quantified.

3. Results and discussions

Fig. 1 provides a series of sintering strains as a function of sintering time for free and constrained films, both of which are sintered at 760 °C, 780 °C and 800 °C, respectively. The true

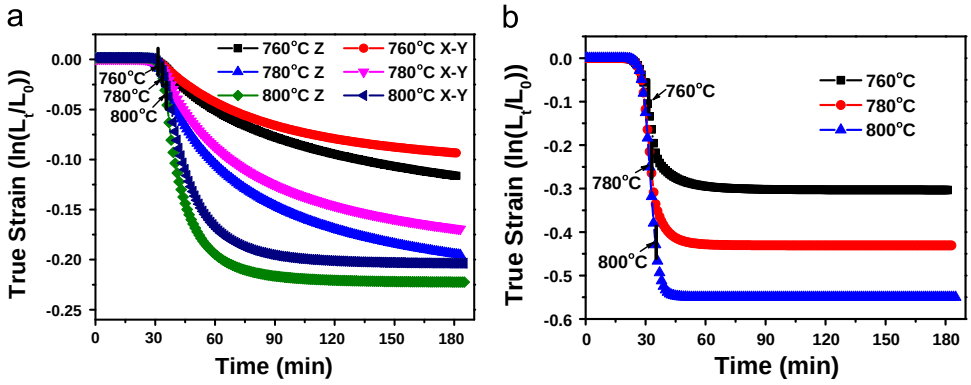

Fig. 1. Sintering strains as a function of sintering time for (a) freely and (b) constrained sintered films sintered at 760 °C, 780 °C and 800 °C.

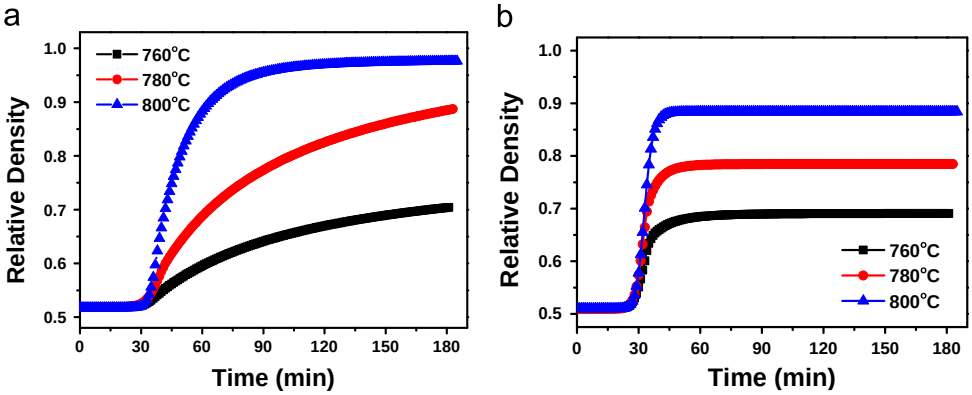

Fig. 2. Relative densities as a function of sintering time for (a) freely and (b) constrained sintered films sintered at 760 °C, 780 °C and 800 °C.

strain definition was used, rather than engineering strains, in the calculation of all sintering strains because of the large deformation involved in sintering; i.e., $\varepsilon = ln(L/L_0)$, where L and L_0 were the instantaneous and initial dimensions in the measuring direction. By assuming an isotropic shrinkage in the in-plane direction, strains for free films were determined through the dimension changes in the in-plane (x–y) and thickness (z) direction. Fig. 1(a) shows the strain curves of free films sintered at different temperatures. The strain in the in-plane (ε_{x-y}) and thickness (ε_z) direction began to decrease at the sintering time of 30 min, corresponding to the temperature of 750 °C. Observably, the strain decreased faster in the isothermal stage and a slight higher shrinkage in the thickness could also be detected, keeping consistent with a recent report [36]. However, shrinkage only occur in the z direction for constrained films and the measured data is shown in Fig. 1(b). It could be seen that ε_z started to decrease at the time of 27 min, corresponding to a lower temperature of 720 °C. The strain decreased rapidly with the sintering time and reached a plateau at the early isothermal stage, indicating that most densification took place during the heating ramp process.

As sintering proceeded, the film density increased and they could be computed through Eqs. (1) and (2) for free and constrained films ($\varepsilon_x = \varepsilon_y = 0$), respectively.

$$\rho = \rho_0 \cdot \exp\left(-2\epsilon_{x-y} - \epsilon_z\right) \quad (1)$$

$$\rho = \rho_0 \cdot \exp(-\epsilon_z) \quad (2)$$

where ρ_0 is the density after the organic burnout at 450 °C, ε_{x-y} and ε_z are the corresponding strains for the sintered films. The density curves as a function of sintering time for free and constrained films are shown in Fig. 2(a) and (b), respectively. It could be seen from Fig. 2(a) that the density increased continuously after 750 °C and final densities for freely sintered films could reach 0.95, 0.88 and 0.70 after sintering at 800 °C, 780 °C and 760 °C, respectively. However, as depicted in Fig. 2(b), the density curve for constrained films evolved in a different way, where the density started to increase after 720 °C and a sharply increasing curve could be observed before reaching the isotheral temperatures. The density of constrained films reached a plateau value at the early isothermal stage, where lower densities of 0.88, 0.78 and 0.69 were obtained after sintering at 800 °C, 780 °C and 760 °C, respectively. The constrained film was cast on a substrate and any dimension changes in the in-plane direction were prohibited during the organic burnout process. Thus, it could be deduced that residual stresses would be induced in the constrained film, which had a negligible effect for the polycrystalline material but remarkable for LTCC. The softening point was around 700 °C for the studied glass ceramic and a glassy state would be obtained when the temperature exceeded 700 °C [26,33]. As the densification process was

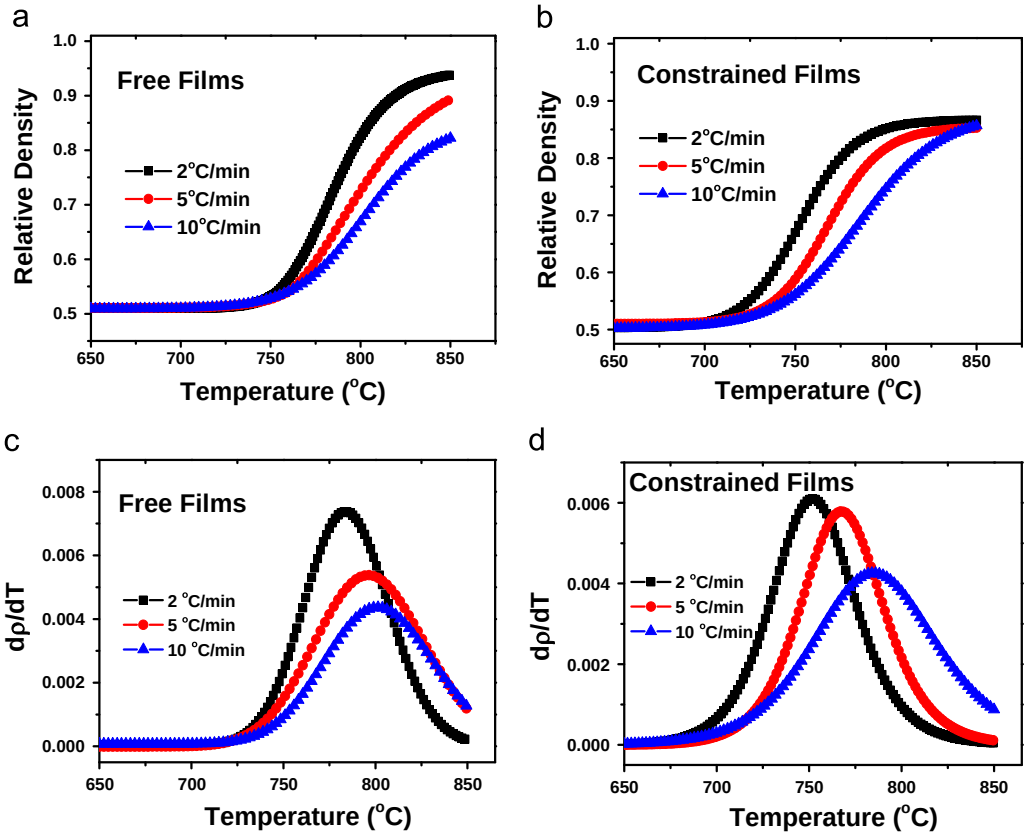

Fig. 3. Curves of density versus sintering temperature for (a) freely and (b) constrained sintered films at different heating rates; (c) and (d) exhibit the density derivatives versus temperature.

mainly conducted through viscous flow and the mass transfer in the sample could be facilitated with a small stress [32]. Therefore, the residual stress remained in the constrained film and the tensile stress from the substrate could modify the densification behavior and the film started to shrink at a lower temperature of 720 °C.

To investigate the influence of substrate on densification kinetics, CHR experiments were carried out for the free and constrain films. The obtained density curves as a function of sintering temperature for free and constrained films are shown in Fig. 3. Evidently, the density increased monotonously with the sintering temperature but grew in different ways for free and constrained films. Owing to the longer soaking time during the CHR experiment, a much steeper density curve could be observed for a low heating rate. Thus, final densities for the freely sintered film were dependent on the sintering rate. However, a similar density around 0.85 could be achieved for constrained films under different heating rates, which was smaller than that sintered at 800 °C. The phenomenon was closely related with the crystallization at temperatures higher than 800 °C, which was usually detrimental to the densification [33]. Derivatives of density with respect to the temperature for free and constrained films sintered at different heating rates are displayed in Fig. 3(c) and (d). It has been demonstrated that the position and the height of the peak in $d\rho/dT$could give an indication of the activation energy [35]. By comparing two sets of curves, it could be seen that the peaks for the constrained films appeared at a much lower temperature, probably due in large part to the residual stress generated in the film.

Then, the activation energies could be calculated by using Eq. (3) as follows [35]:

$$\ln\left(T\dot{T}\frac{\mathrm{d}\rho}{\mathrm{dT}}\right) = -\frac{Q}{\mathrm{RT}} + \ln(f(\rho)) \tag{3}$$

where T and $\dot{T}$ are the absolute temperature and the heating rate in CHR experiments. The apparent activation energy could be determined from the slop of fitted straight lines. As shown in Fig. 4(a), the fitted lines are almost parallel to each other and a relatively fixed value of 530 ± 30 kJ/mol could be obtained for freely sintered films when the density increased from 0.55 to 0.85. However, as observed in Fig. 4(b), the activation energy for the constrained film decreased from 670 kJ/mol to 359 kJ/mol as the density increased from 0.55 to 0.85. As mentioned above, the residual stress originated from the binder burnout process might give rise to the higher activation energies in the early densification stage of constrained films. With increasing density values, the residual stress was released by viscous flow, resulting in a decrement of the sintering activation energy. Moreover, owing to the constraint from the rigid substrate, the shrinkage was allowed only in the thickness direction, leading to a further decrease in the activation energy.

Our results has revealed that the densification behavior of constrained films were quite different from that of freely sintered films. First, the starting densification temperature for

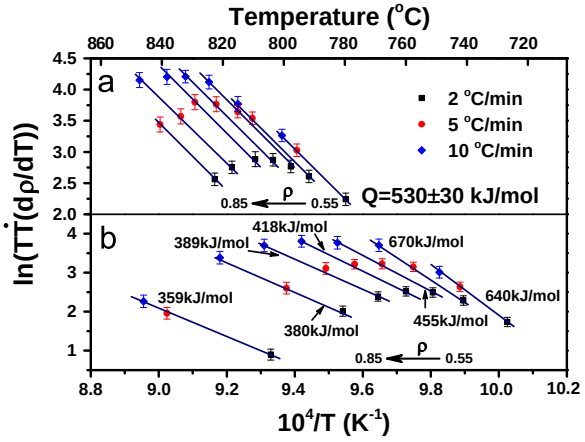

Fig. 4. Plots for the estimation of activation energies for (a) freely and (b) constrained sintered films using the method described in the text. The tolerances for the activation energies in (a) reflect the slight change in the slope at different values of the density.

the constrained film was around 720 °C, which was 30 °C lower than that of the freely sintered films. During the organic burnout process, the movement of particles in the constrained film was not allowed and residual stress could be generated in the film, which was usually induced by the fierce release of gas generated in the reaction [35]. The residual stress could only be eliminated through the mass transfer in the film. It has been demonstrated that the present studied LTCC material firstly densified based on viscous flow and then crystallized at temperatures higher than 800 °C [33]. It has been clearly proved that Ca–B–Si based glass ceramic would change into the glassy state when the temperature was above 700 °C and the presence of the silica particles in a borosilicate glass decreased the limit of densification rate when the film was constrained [18,19,27,33]. Additionally, it has been well documented that the viscosity of the LTCC materials was relatively low and decreased with increasing sintering temperature [33]. Shear response was reported to be a main feature

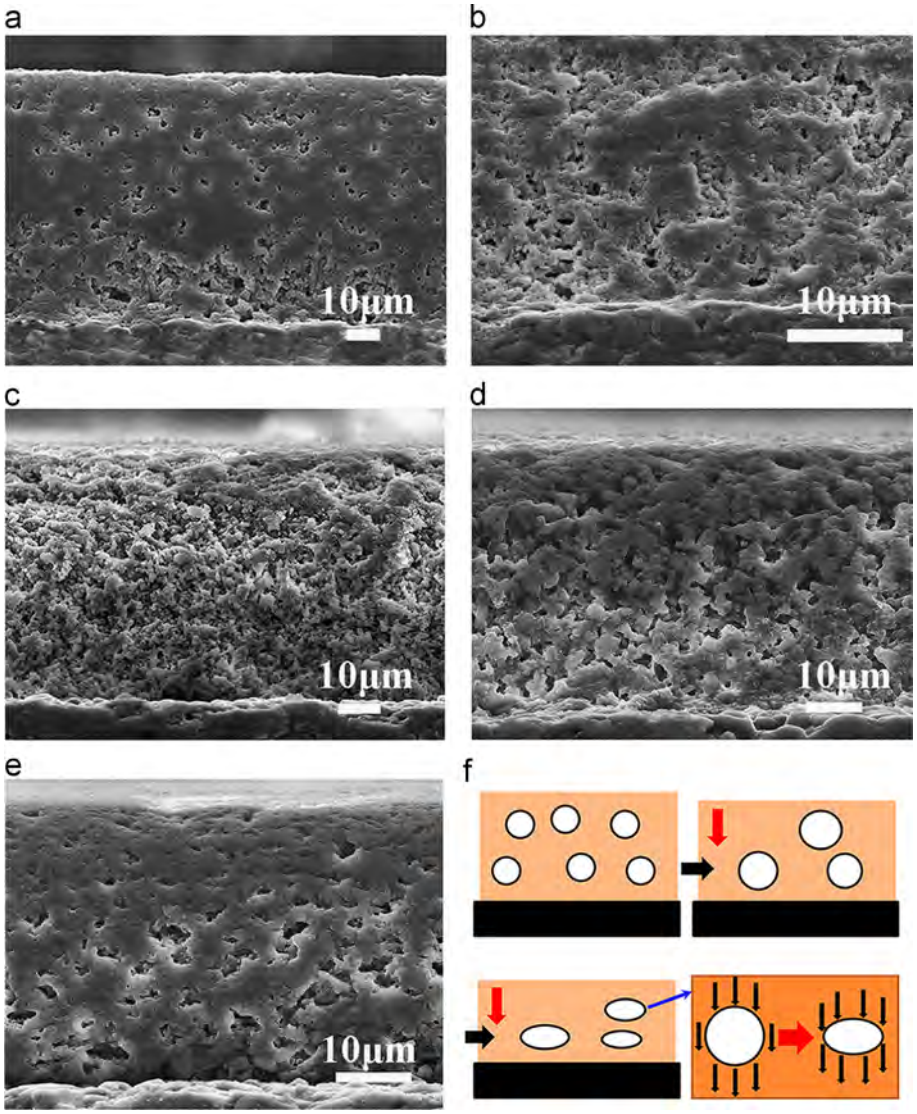

Fig. 5. Polished cross-section of constrained films (130 μm) sintered at 780 °C for 2 h: (a) and (b) the interfacial morphology with different magnifications, and films (70 μm) isothermally sintered at 780 °C for (c) 0 min, (d) 10 min, (e) 120 min and (f) sketch image for the pore evolution rule.

for the constrained films [15]. The stress could be released through the quick shear response of the glass-ceramic, since the viscosity decreased with increasing temperatures. Thus, the shrinkage of the constrained film in the thickness direction was facilitated by the stress and it was detectable that the density of the constrained film exhibited a more rapid growth when compared with the freely sintered films at heating ramp stage. Thus, the sintering activation energy of constrained films in the early densification stage was much higher than that of free films, which could be mainly assigned to the residual stress in the film. After the release of residual stress, the activation energy decreased with the increase of density and the activation energy for constrained films was much lower than that of free films at densities higher than 0.65.

The interface between the film and the substrate is important for the analysis of sintering kinetics. During the sintering process, the connection between the substrate and the film was strong enough, which could hinder the shrinkage of the film in the in-plane direction without any observable defects. And the changes in the densification kinetics could be mainly attributed to the constraining stress from the substrate. The microstructure at the interface was characterized for the film sintered at 780 °C and the images are displayed in Fig. 5 (a) and (b). A good bonding can be observed between the film and the substrate, except for some pores at the interface, which could be assigned to the inner stress from the substrate [5,20,28]. Owing to the strong bonding with the substrate, particles in the film are not allowed to move along the in-plane direction during the sintering process. The studied film is a glass-ceramic system material with a glass temperature around 750 °C [33]. The densification process was mainly realized through the viscous flow, which was faster at a higher temperature [32]. Owing to the existence of the inner stress, the hindering effect for the viscous flow was much higher at the interface than that at the free surface. As the densification proceeded, pores away from the interface could be fast eliminated through the viscous flow, but those at the interface were not easy to be removed, thus leading to a porosity gradient

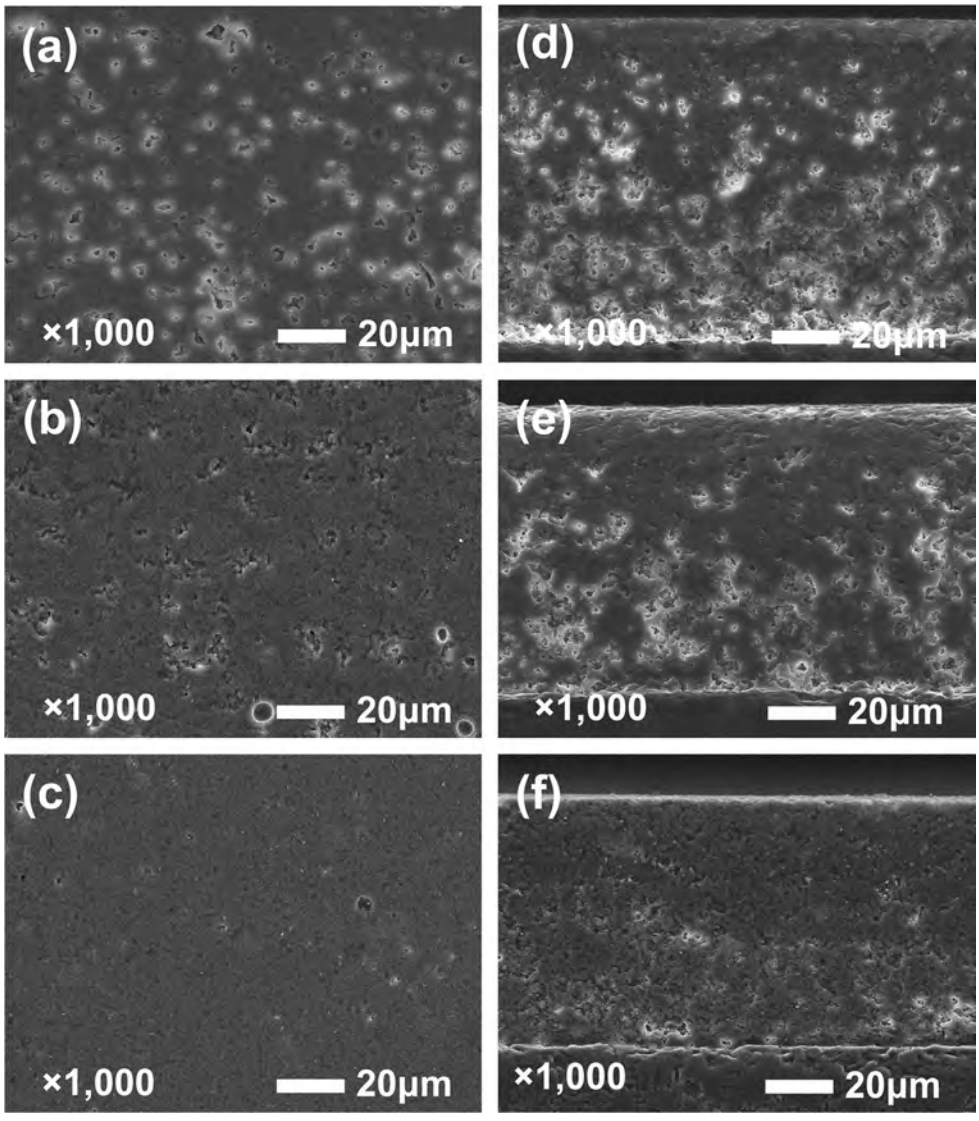

Fig. 6. Polished cross-section of sintered films: freely sintered films at (a) 760 °C, (b) 780 °C and (c) 800 °C, and constrained films sintered at (d) 760 °C, (e) 780 °C and (f) 800 °C.

in the thickness direction. Moreover, larger pores could also be observed at the interface, which could be clearly observed in Fig. 5(a). Owing to the strong inner stress at the interface, no mass transfer could occur in the in-plane direction, the pore shrinkage could only be achieved by the viscous flow in the thickness direction and pores became more elliptical, as depicted in Fig. 5(b).

It has been demonstrated that anisotropy and heterogeneity in the microstructure would occur in constrained films and more severe anisotropy could be observed with the decrease of film thickness [2,20–24,28–30]. As for constrained polycrystalline films, pores were prone to align perpendicular to the substrate, which was the result of the altered mass transfer route. The present studied LTCC films were densified based on a viscous flow and the anisotropy evolution in LTCC materials were quite different from that of polycrystalline ceramics [2,32]. The microstructure evolution under compressive stresses in LTCC bulk materials has been illustrated in several reports [1,2,27]. And it was of necessity to understand the microstructure evolution in the substrate-constrained LTCC films. Herein, films with a thickness of 70 μm were firstly utilized to explore the potential anisotropy evolution law. The films were sintered at 780 °C for 0, 10 and 120 min and their corresponding SEM images in the *y*–*z* plane are shown in Fig. 5(c), (d) and (e), respectively. The comparison among the images demonstrated a decrement in the thickness and the overall porosity. When the temperature just reached 780 °C, the porosity was high and no pore orientation could be detected, as manifested by Fig. 5(c)–(e) indicated that with prolonging the isothermal time, the pores became slight larger than that in Fig. 5(c) after carefully measuring the pore's axes. Moreover, elongated pores along the direction parallel to the substrate could be conspicuously detected in Fig. 5(e). On the basis of the viscous flow mechanism, rules responsible for the anisotropy evolution can be proposed and the sketch image was graphically displayed in Fig. 5(f).

To get a deep understanding of the evolved anisotropy, quantitative analysis for free and constrained films (130 μm) sintered at 760 °C, 780 °C and 800 °C were conducted. The corresponding images for the freely sintered samples are shown in Fig. 6(a), (b) and (c), respectively. Obviously, the porosity decreased with increasing sintering temperature. Pores were evenly distributed and most pores exhibited a nearly circular morphology, showing a typical isotropic feature. Moreover, the microstructure of free films resembled that of polycrystalline materials with sharp boundaries among particles, which matched well with previous observation [1]. The cross-sections of constrained films sintered at 760 °C, 780 °C and 800 °C are shown in sequence from Fig. 6(d) to (f). In contrast to free films, a higher porosity was observed in the constrained films. And the porosity was found to become lower with the increase of the distance away from the interface, which could be by virtue of the fact that in-plane tensile stress reached its maximum at the interface and gradually disappeared close to film surface [29]. Therefore, the evolved porosity gradient in constrained films was a clear indication for the evolved anisotropy and further

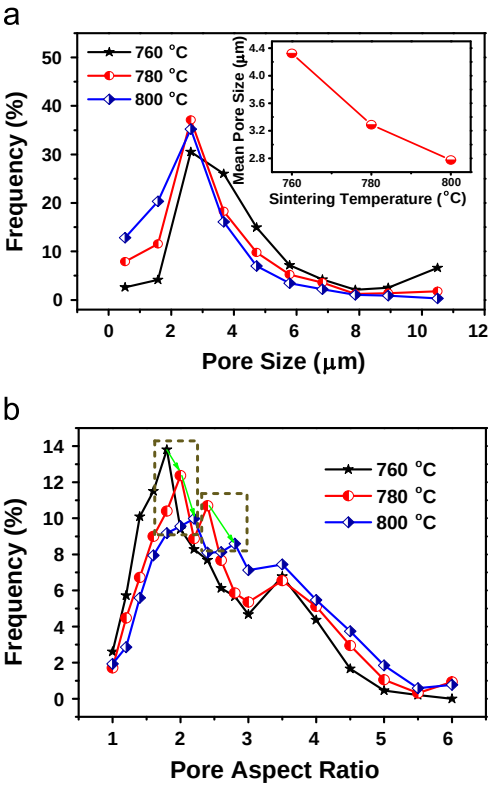

Fig. 7. (a) Pore size distribution and (b) pore aspect ratio of constrained films sintered at different temperatures.

quantitative analyses on the pores were conducted by characterizing the size, shape and orientation.

Fig. 7 displays the pore size and aspect ratio distributions of constrained films. For characterization, equivalent ellipses were acquired for the elongated pores and their major axes were taken as the characteristic length. As shown in Fig. 6(a), the pore size exhibited a unimodal distribution with the peak locating at about 2.5 μm for films sintered at 760 °C. An increased frequency of pores smaller than 2 μm could be yielded with increasing sintering temperature. The mean pore size reduced with the increase of sintering temperatures, as could be clearly seen through the inset figure. The aspect ratio for elongated pores is an important factor in revealing the anisotropy [28,29]. Then, pore aspect ratios for the constrained films are determined and shown in Fig. 6(b). As displayed in the figure, the pore aspect ratio exhibited a bimodal or trimodal distribution. For the constrained film sintered at 760 °C, a bimodal distribution of the pore aspect ratio could be observed with peaks lying at 1.8 and 3.5. However, aspect ratio distributions evolved from bimodal to trimodal with the increase of sintering temperature. For constrained films sintered at 780 °C, the three peaks lied at 2, 2.4 and 3.5, respectively. By further elevating the sintering temperature to 800 °C, the second peak shifted to the ratio of 2.8. The frequency for highly elongated pores (aspect ratio above 3) increased from 13% to 25% as the sintering temperature elevated from 760 °C to 800 °C. The evolution of pore aspect ratio clearly revealed that pores became more anisometric as densification proceeded.

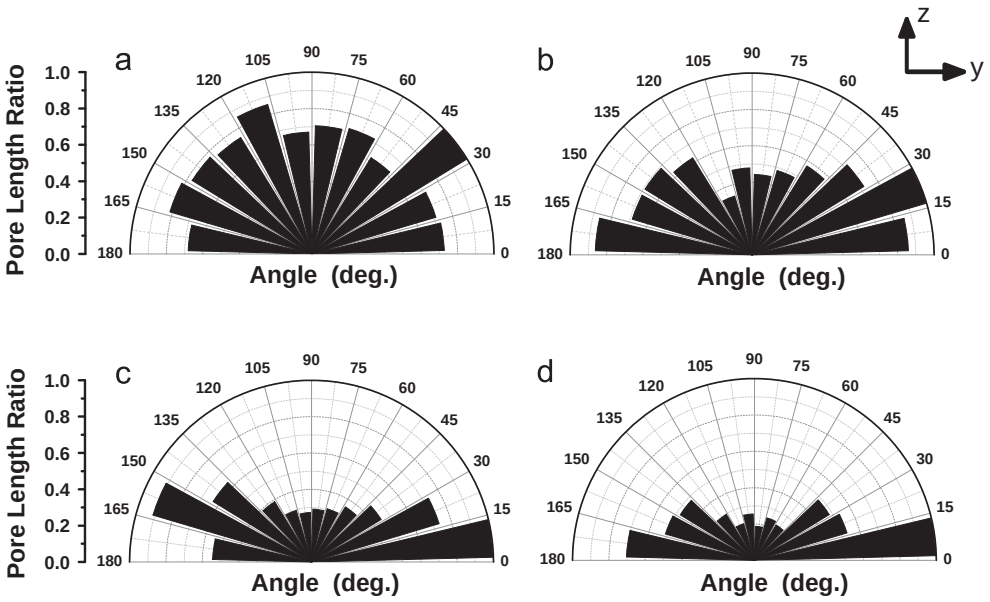

Fig. 8. Cumulated weighted length of pores in the *YZ*-plane for (a) free film sintered at 780 °C and constrained films sintered at (b) 760 °C, (c) 780 °C and (d) 800 °C.

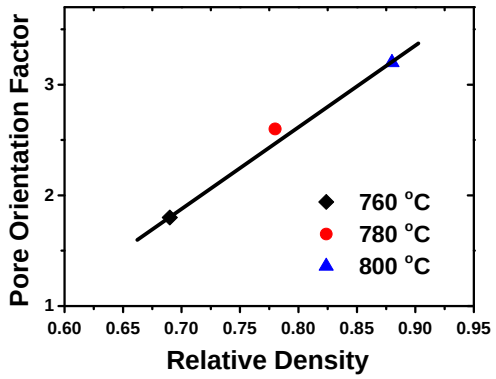

Fig. 9. Pore orientation factor in *YZ*-plane for constrained films at different density.

The pore orientation can be further evaluated by cumulating pore length lying in a defined angle range. In order to differentiate pores with same length but different degrees of anisotropy, we decided to multiply the pore length by its aspect ratio to give a higher weight to pores that were more elliptical. Finally, the results were normalized with the maximal measured value. The obtained polar plots for free film sintered at 800 °C and constrained films sintered at 760 °C, 780 °C and 800 °C are displayed in Fig. 8(a), (b), (c) and (d), respectively. As shown in Fig. 8(a), pores are randomly orientated in free films. However, pores were more or less randomly distributed with slight tendency to align parallel to the substrate, as displayed in Fig. 8(b). Furthermore, with the increase of sintering temperature, pores were more prone to align parallel to the substrate direction, which could be detected from Fig. 8(c) to (d). Thus, anisotropic microstructure with pores aligning parallel to the substrate was obtained with the increase of density.

In order to quantify the evolved anisotropy, the following pore orientation factor was introduced, which was determined by the ratio of the cumulated weighted length measured in the thickness direction (between 60° and 120°) and that in the in-plane direction (between 0° and 30°, as well as between 150° and 180°). The obtained results are shown in Fig. 9, where a continuous development of anisotropy can be observed. It could be seen that the orientation factor for the constrained film increased from 1.8 to 3.2 as the density increased from 0.69 to 0.88. A more than 77% increase of the initial orientation factor indicated an obvious anisotropy development as a function of density. By extrapolating the curve, a higher degree of anisotropy was expected for almost fully densified films as well as values close to 1 for green density about 57%.

As widely known, the microstructure evolution of constrained films is closely related with their densification mechanism. The studied LTCC constrained films were densified based on viscous flow. As revealed in our results, pores in constrained films were prone to aligned parallel to the substrate with the increase of density. Due to the biaxial tensile stress from the substrate, only thickness changes were allowed in the constrained film. Therefore, the mass transfer in the thickness direction was promoted, contributing to a larger shrinkage in the direction [36]. And elongated pores aligned parallel to the substrate were formed as densification proceeded.

4. Conclusions

The densification behavior of free and constrained LTCC films sintered at different temperatures was investigated by means of a lab-made optical dilatometer. A CHR experiment was conducted to determine the apparent activation energy. The microstructure of free and constrained films was carefully examined in order to validate the anisotropy evolution. The results were summarized as follows:

(1) The starting densification temperature was 720 °C for the constrained film, which was lower than that for free films.
(2) The density for constrained films increased quickly at the heating and early isothermal stage. And the final density was lower than that of free films, which could be mainly attributed to the constraint from the substrate.
(3) The apparent activation energy was determined to be 530 ± 30 kJ/mol for freely sintered films throughout the sintering process. But it decreased from 690 kJ/mol to 359 kJ/mol for constrained films with the increase of density.
(4) Anisotropic microstructure was evolved in constrained films and pores were more prone to align parallel to the substrate.

Acknowledgments

This work was financially supported by a Project of the National Natural Science Foundation of China (51272060).

References

[1] A. Mohanram, G.L. Messing, D.J. Green, Densification and sintering viscosity of low-temperature co-fired ceramics, J. Am. Ceram. Soc. 88 (2005) 2681–2689.
[2] J.B. Ollagnier, O. Guillon, J. Rödel, Effect of anisotropic microstructure on the viscous properties of an LTCC material, J. Am. Ceram. Soc. 90 (2007) 3846–3851.
[3] R.Z. Zuo, E. Aulbach, J. Rödel, Shrinkage-free sintering of low-temperature cofired ceramic by loading dilatometry, J. Am. Ceram. Soc. 87 (2004) 526–528.
[4] J.B. Ollagnier, O. Guillon, J. Rödel, Viscosity of LTCC determined by discontinuous sinter-forging, Int. J. Appl. Ceram. Technol. 3 (2006) 437–441.
[5] T. Cheng, R. Raj, Flaw generation during constrained sintering of metal-ceramic and metal-glass multilayer films, J. Am. Ceram. Soc. 72 (1989) 1649–1655.
[6] J.W. Chow, J.N. Calat, G.Q. Lu, Constrained film sintering of a gold circuit paste, J. Mater. Res. 10 (1995) 986–994.
[7] Y.C. Lin, J.H. Jean, Constrained sintering of silver circuit paste, J. Am. Ceram. Soc. 87 (2004) 187–191.
[8] J.H. Jean, C.R. Chang, Camber development during cofiring Ag-based low-dielectric-constant ceramic package, J. Mater. Res. 12 (1997) 2743–2750.
[9] A. Mohanram, S.H. Lee, G.L. Messing, D.J. Green, Constrained sintering of low-temperature co-fired ceramics, J. Am. Ceram. Soc. 89 (2006) 1923–1929.
[10] J. Ollagnier, O. Guillon, J. Rödel, Constrained sintering of a glass ceramic composite: I. asymmetric laminate, J. Am. Ceram. Soc. 93 (2010) 74–81.
[11] M. Hambuch, A. Roosen, Joining of sintered alumina substrates and LTCC green tapes via cold low-pressure lamination, Int. J. Appl. Ceram. Technol. 11 (2014) 443–450.
[12] R.K. Bordia, G.W. Scherer, On constrained sintering-I constitutive model for a sintering body, Acta Metall. 36 (1988) 2393–2397.
[13] R.K. Bordia, G.W. Scherer, On constrained sintering-II comparison of constitutive models, Acta Metall. 36 (1988) 2397–2409.
[14] D.J. Green, O. Guillon, J. Rödel, Constrained sintering: a delicate balance of scales, J. Eur. Ceram. Soc. 28 (2008) 1451–1466.
[15] R.K. Bordia, R. Raj, Sintering behavior of ceramic films constrained by a rigid substrate, J. Am. Ceram. Soc. 68 (1985) 287–292.
[16] T.J. Garino, H.K. Bowen, Deposition and sintering of particle films on a rigid substrate, J. Am. Ceram. Soc. 70 (1987) C-315–C-317.
[17] G.W. Scherer, T. Garino, Viscous sintering on a rigid substrate, J. Am. Ceram. Soc. 68 (1985) 216–220.
[18] J. Bang, G.Q. Lu, Densification kinetics of glass films constrained on rigid substrates, J. Mater. Res. 10 (1995) 1321–1326.
[19] J. Bang, G.Q. Lu, Constrained-film sintering of a borosilicate glass: in situ measurement of film stress, J. Am. Ceram. Soc. 78 (1995) 813–815.
[20] O. Guillon, E. Aulbach, J. Rödel, Constrained sintering of alumina thin films: comparison between experiment and modeling, J. Am. Ceram. Soc. 90 (2007) 1733–1737.
[21] J.S. Kim, R.A. Rudkin, X. Wang, A. Atkinson, Constrained sintering kinetics of 3YSZ films, J. Eur. Ceram. Soc. 31 (2011) 2231–2239.
[22] J.N. Calat, G.Q. Lu, T.J. Chuang, Constrained sintering of glass, glass-ceramic and ceramic coatings on metal substrates, Surf. Interface Anal. 31 (2001) 673–681.
[23] T.J. Garino, H.K. Bowen, Kinetics of constrained-film sintering, J. Am. Ceram. Soc. 73 (1990) 251–257.
[24] R.K. Bordia, R.Z. Zuo, O. Guillon, S.M. Salamone, J. Rödel, Anisotropic constitutive laws for sintering bodies, Acta Mater. 54 (2006) 111–118.
[25] A. Mohanram, G.L. Messing, D.J. Green, Measurement of viscosity of densifying glass-based systems by isothermal cyclic loading dilatometry, J. Am. Ceram. Soc. 87 (2004) 192–196.
[26] R.J. Xie, R.Z. Zuo, E. Aulbach, U. Mackens, N. Hirosaki, J. Rödel, Uniaxial viscosity of low-temperature cofired ceramic (LTCC) powder compacts determined by loading dilatometry, J. Eur. Ceram. Soc. 25 (2005) 417–424.
[27] J.B. Ollagnier, D.J. Green, O. Guillon, J. Rödel, Constrained sintering of a glass ceramic composite: II. symmetric laminate, J. Am. Ceram. Soc. 92 (2009) 2900–2906.
[28] O. Guillon, L. Weiler, J. Rödel, Anisotropic microstructural development during the constrained sintering of dip-coated alumina thin films, J. Am. Ceram. Soc. 90 (2007) 1394–1400.
[29] O. Guillon, S. Krauß, J. Rödel, Influence of thickness on the constrained sintering of alumina films, J. Eur. Ceram. Soc. 27 (2007) 2623–2627.
[30] C.L. Martin, R.K. Bordia, The effect of a substrate on the sintering of constrained films, Acta Mater. 57 (2009) 549–558.
[31] R.Z. Zuo, E. Aulbach, R.K. Bordia, J. Rödel, Critical evaluation of hot forging experiments: case study in alumina, J. Am. Ceram. Soc. 86 (2003) 1099–1105.
[32] S. Kemethmüller, M. Hagymasi, A. Stiegelschmitt, A. Roosen, Viscous flow as the driving force for the densification of low-temperature co-fired ceramics, J. Am. Ceram. Soc. 90 (2007) 64–70.
[33] C.R. Chang, J.H. Jean, Crystallization kinetics and mechanism of low-dielectric, low-temperature, cofirable $CaO–B_2O_3–SiO_2$ glass-ceramics, J. Am. Ceram. Soc. 82 (1999) 1725–1732.
[34] L.P. Yu, S.S. Qi, Z.S. Ma, R.Z. Zuo, Experimental determination of the uniaxial viscosity of low-temperature co-fired ceramic tapes by vertical sintering, Ceram. Int. 40 (2014) 9367–9375.
[35] J. Wang, R. Raj, Estimate of the activation energies for boundary diffusion from rate-controlled sintering of pure alumina, and alumina doped with zirconia or titania, J. Am. Ceram. Soc. 73 (1990) 1172–1175.
[36] C.S. Ni, J.T.S. Irvine, Image analysis and modeling of the orientation of pores in a constrained film on a rigid substrate, J. Am. Ceram. Soc. 98 (2015) 2403–2410.